Instrumentation for ac four-probe measurements of large impedances

G. Fafilek *, M.W. Breiter

Institut für Technische Elektrochemie, TU Wien, Getreidemarkt 9, A-1060 Vienna, Austria

Abstract

An ac four-probe set-up was constructed to measure impedance spectra between 1 Hz and 100 kHz on solid electrolytes up to impedance values of 10 GΩ. The influence of the system on the measurement was analysed for the previous and the new set-up. A solution to minimise the source of errors by pre-amplifiers for current and voltage signals is presented. A new sample holder was constructed for best results in conjunction with the new pre-amplifiers. The holder is designed for measurements on solid electrolytes over a wide temperature range. The performance of the improved set-up and the residual error sources are discussed. Measurements of impedance spectra on YSZ and BICUVOX.10 in a four-probe arrangement are given as an example. © 1997 Elsevier Science S.A.

1. Introduction

Impedance spectroscopy on symmetric cells by two-probe techniques is widely used for the measurement of bulk impedances in solid state ionics. The disadvantage is the necessary separation of the bulk impedance from the interfacial impedance bulk|electrode. This is sometimes difficult. On the other hand, the impedance spectra allow a distinction to be made between different bulk processes, such as intragranular and intergranular conduction in polycrystalline material [1]. The four-probe technique avoids the difficulties of the separation of interfacial impedances because only the voltage drop across the bulk impedance between the two voltage probes is measured [2]. Since current and voltage probes are separated and, in theory, current does not pass through the voltage electrodes, the voltage drop across the part of the electrolyte between the voltage probes should be measured without contribution of the impedance of the bulk|electrode interface.

Usually dc or fixed frequency systems are used as standard methods [3]. However, only the total resistivity can be determined by these methods. Although impedance spectra can be taken, their interpretation is very difficult in many cases. Correct results are only obtained for systems with low resistance (less than approximately 1 MΩ). The

measurement is restricted to a relatively small frequency range (less than 1 kHz) [4,5]. Systems with very high impedance cannot be measured by standard methods because of the influence of the set-up. Even though interfacial properties should not contribute to the measurement, in practice there is a voltage drop at the interfacial impedance of the voltage probes. Bias currents to the amplifier inputs, the cable capacity and the input impedance of the amplifier, are loads for the probes and form current paths across that part of the bulk impedance where the voltage drop is measured. The size of the voltage probes is one of the parameters which determines the value of the interfacial impedance. Therefore the area cannot be too small but, on the other hand, large probes disturb the uniformity of the current distribution.

In this paper we describe the reasons for these errors and discuss the possibilities for reducing these problems.

2. Equivalent circuit of the ac four-probe set-up

In a four-probe set-up, stray capacities have more influence on the measurements than in a two-probe set-up. A schematic diagram of a traditional four-probe set-up is shown in Fig. 1. For this arrangement the ac response of the system can be evaluated by equivalent circuits. A complicated equivalent circuit, which is shown in Fig. 2, results because the impedance of the sample outside of the voltage probes cannot be neglected. This model may be

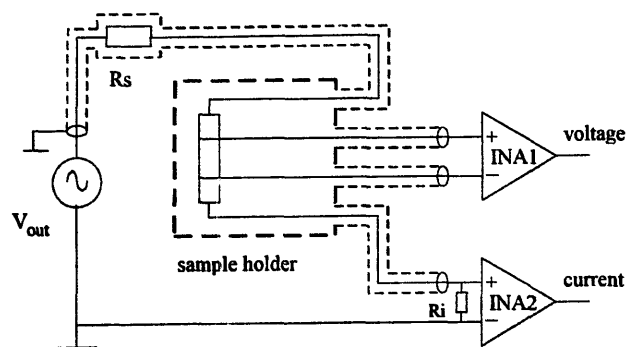* Corresponding author. Fax: 0043 1 5861560. E-mail: sekrl58@fbch.tuwien.ac.at.
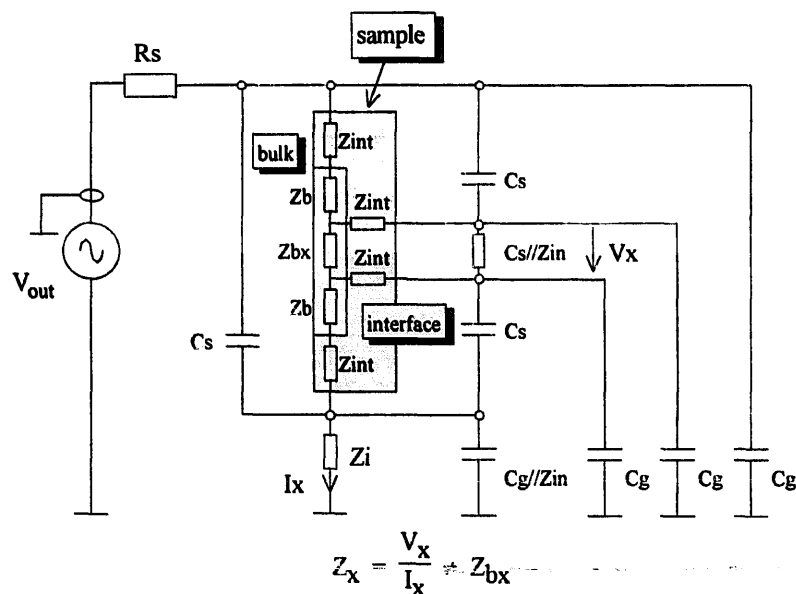
Fig. 1. Schematic diagram of the set-up for conventional measurement of voltage and current. Both are measured with the same type of instrumentation amplifier.

too simple to simulate the real behaviour of the set-up because the values of the different parameters are not known exactly. However, this circuit can show qualitatively why it is so difficult to get correct results for the impedance to be measured. The stray capacity across a large standard resistor for the current measurement leads to a decreased bandwidth in the voltage drop technique. Stray capacities of the voltage leads and the input impedance of the voltmeter also produce a bypass to the unknown impedance and contribute to the measured current. In

addition the frequency response of the amplifiers has to be considered. It is therefore necessary to modify the measuring circuits used commonly for ac four-probe measurements of high impedance systems.

In ac two-probe measurements, the use of a current-to-voltage converter instead of the measurement of the voltage drop across a standard resistor is a common method to avoid stray capacities. With that arrangement the ac performance of the current measurement depends mainly on the performance of the amplifier and very large impedances can be measured [6]. A similar technique can be used in the four-probe set-up. The schematic diagram of the new set-up is shown in Fig. 3a. A current to voltage converter instead of a standard resistor in series with the sample and a voltage amplifier which allows the use of driven shields [7] was implemented. The equivalent circuit in Fig. 3b is simpler than that in Fig. 2. The capacity, C_g, and the impedance, Z_{in}, formed by the cable and the amplifier input do not influence the measurement because of the virtually grounded input of the current-to-voltage amplifier. The cable capacity, C_g, to the ground of the voltage leads, and the stray capacity, C_s, between the voltage signal leads, can be eliminated by the active shielding. It is necessary to extend the active shield as close as possible to the sample even at high temperatures. The current leads

$$Z_x = \frac{V_x}{I_x} \neq Z_{bx}$$

Z_{int}	impedance of the bulk|electrode interface
Z_b	impedance of the bulk
Z_{bx}	impedance to be measured
C_s	stray capacity between signal lines
Z_{in}	input impedance of amplifier
C_g	capacity between signal line and grounded shield
Z_i	standard resistor
V_x	measured voltage drop
I_x	measured current
Z_x	measured impedance

different from real values

Fig. 2. Equivalent circuit of the set-up shown in Fig. 1.

should have grounded shields up to the current probes of the sample. Therefore a stray capacity cannot be formed from these lines to other signal lines. The cable capacity C_g of the high current input lead, which still exists, will not influence the measured impedance. Only the input impedance of the instrumentation amplifier in parallel to the sample remains. This would be the ideal behaviour of the circuit. The value of the input capacity, which is usually between 1 and 2 pF, can be taken into account in the calculation of the real bulk impedance, Z_{bx}, from the measured impedance, Z_x:

$$Z_x = \frac{V_x}{I_x} = \frac{Z_{in}Z_{bx}}{Z_{in} + Z_{bx} + 2Z_{int}} \quad (1)$$

In Eq. (1), derived from the circuit in Fig. 3b, the interfacial impedance of the voltage electrodes has to be included. That is the reason why in the four-probe measurement, even when it is made by a carefully designed set-up, the interfacial impedance contributes to the total impedance. One has to make a compromise between geometric effects due to the non-uniform current distribution

for large voltage probes and interfacial effects for small electrodes.

3. Description of the set-up

A previously described set-up for computer controlled four-probe measurements [2] was modified to allow the measurement of larger impedances in a wider frequency range. Amplifiers and sample holder were newly constructed for that purpose.

3.1. Voltage amplifier

An instrumentation amplifier can measure voltage differences floating to the ground, which is required for the measurement of the potential drop across the voltage probes. The amplifier inputs have to be connected to the sample through shielded cables. The capacitive coupling between noise sources, mostly from the power line, and the signal line, introduces noise [8]. The noise current
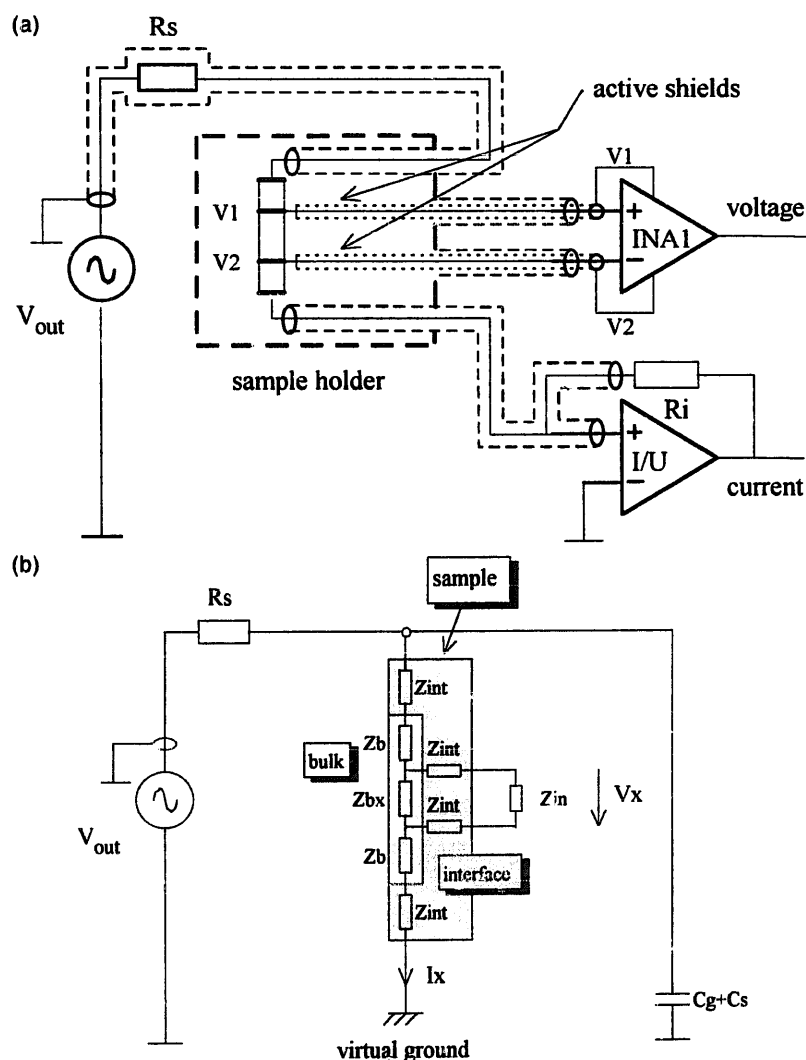

Fig. 3. (a) Schematic diagram of the four-probe set-up with special current and voltage amplifier. (b) Resulting equivalent circuit.

flows through the shield, not through the signal line with a grounded metal shield. However, the cable capacity C_g and the leakage resistance R_g from the signal line to the grounded shield are loads for signal sources with large source impedance. To avoid this influence, active shielding is necessary. The active shield is held at the same signal level as the signal line itself by means of a buffer amplifier. In principle, active shielding (guarding) rejects the capacitive current even when the cable capacity still exists. The performance of the guarding depends on the performance of the buffer amplifier. The frequency dependence of the open loop voltage gain has a single pole behaviour. Therefore the voltage difference between signal line and guard becomes larger at higher frequencies. Also, the output resistance of the buffer amplifier has some influence on the efficiency of the guarding. The output resistance is normally approximately 100 Ω and forms a low-pass with the capacity between active and grounded

shield in a TRIAX cable. The time constant of this low-pass is very small and the influence on the bandwidth of the whole circuit can be neglected.

3.1.1. The voltage amplifier circuit (Fig. 4a)

An INA 110 instrumentation amplifier from Burr Brown was used for amplification of the voltage signal. This amplifier provides a flat voltage gain–frequency response up to 100 kHz with a gain of 1 or 100. Buffer amplifiers for both inputs, built by the OPA 128 from Burr Brown, ensure the very low bias current of 75 fA, which is necessary to avoid dc-offset on the voltage electrodes [9]. A careful arrangement is necessary to avoid the degrading of the very good performance of this amplifier. Therefore the noninverting inputs of the OPA 128 were directly attached to the TRIAX connectors mounted on the case. The outputs of these buffers also supply the driven shields of the TRIAX cables which are connected to the TRIAX

a)

Voltage amplifier 4-probe

Current amplifier 4-probe

all switches shown in off position
open circles -- off
filled circles -- on

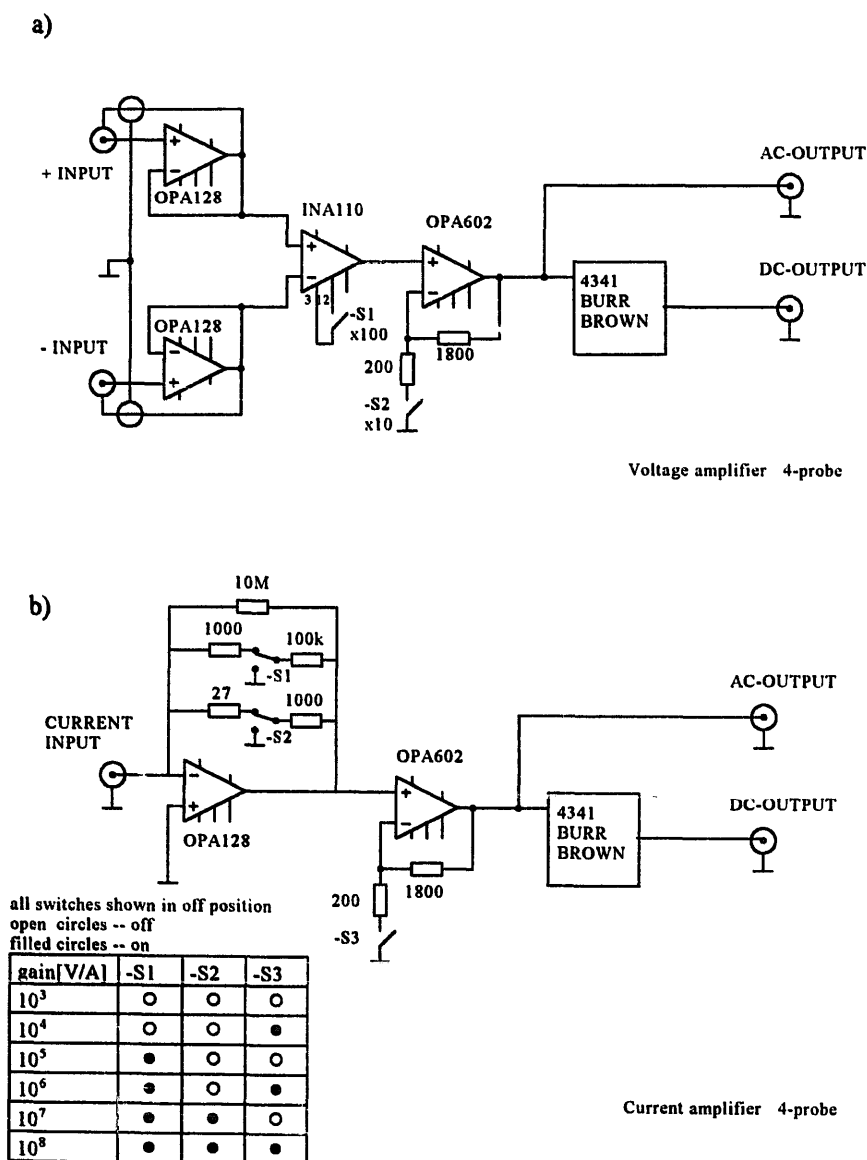| gain[V/A]	-S1	-S2	-S3
10^3	O	O	O
10^4	O	O	●
10^5	●	O	O
10^6	●	O	●
10^7	●	●	O
10^8	●	●	●

Fig. 4. Electronic circuits for (a) voltage and (b) current amplifier. Power supply and offset compensation of the amplifiers are not drawn.

connectors on the sample holder. An additional noninverting amplifier stage (OPA 602, Burr Brown) provides gains of 1 and 10. Together with the INA 110, the gains 1, 10, 100 and 1000 can be set by two relays. A true RMS converter (4341 from Burr Brown) gives additional information about dc-offset, or saturation of the voltage inputs in case of high interfacial impedance or blocking behaviour of the electrodes. The ac output can be used to supply a regular FRA or, in our case, the HP gain-phase meter 3575A was used.

3.2. Current to voltage converter

The same amplifier which is used as a buffer in the voltage amplifier is located in the current-to-voltage converter. The single pole transfer function of the amplifier, together with the low pass, formed by the feedback resistor and the capacity of the input cable of the current amplifier, leads to a two-pole behaviour and introduces gain peaking followed by a -40 dB/dec slope [10]. To avoid gain peaking and oscillation a parallel capacitor across the feedback resistor is required sometimes, reducing the bandwidth.

The voltage applied to the sample is more or less constant, except for impedances smaller than 100 Ω. Therefore the dynamic range of the voltage to be measured, compared to the current, is much smaller. In order to cover a wide range of impedance values it is necessary to have several ranges for the current measurement. Unfortunately, ordinary switching of the ranges in the current to voltage amplifier introduces additional stray capacities in the high gain ranges and therefore additional limitations of the bandwidth. For that purpose a circuit was developed which avoids this influence of the switches on the measurement.

3.2.1. The current amplifier circuit (Fig. 4b)

The OPA 128 was used as a current-to-voltage converter. The switching of the ranges is a difficult problem because of the stray shunting capacities across the feedback resistor. A 10 MΩ feedback resistor was connected directly from the input to the output in such a way that a minimum shunt capacity results. The resistors for the additional ranges were added afterwards. Only a shunt capacity across the feedback resistor will reduce the bandwidth. Stray capacities from the output of the amplifier to ground or from the input (which is practically on virtual ground if the frequency is not too high) to ground have no influence on the bandwidth. If the feedback resistor with low resistance is connected to the output and switched to ground when a higher gain is necessary, only a very small additional stray capacity (compared to the cable capacity) from the input to ground is inserted. The output of the amplifier is loaded by that part of the feedback resistor which is connected to ground. It is about 1000 Ω in the worst case when -S1 and -S2 are switched on. The output
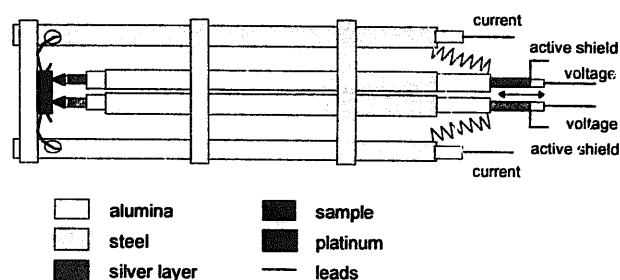

Fig. 5. Sample holder for measurements at high temperatures with point electrodes as voltage probes and active shielding up to the sample.

resistance of 100 Ω and the maximum output current of 5 mA of the OPA 128 have to be considered for accuracy and large signal frequency response characteristics. The second stage of the current amplifier, as well as the true RMS converter, is the same as that in the voltage amplifier.

3.3. Sample holder

The sample holder for measurements at high temperatures (Fig. 5), consists of alumina and steel tubes and platinum leads. The voltage leads had to be actively shielded separately by their own signal potential and were therefore arranged in a triaxial configuration. Both voltage signal leads are isolated by alumina tubes, which are covered by silver paste on the outside. This silver layer is used as an active shield for the high temperature part of the holder. Additional alumina tubes isolate the active shields against the grounded steel tubes. The outer and the inner alumina tubes are glued together and can move inside the steel tubes. On the end where the sample is placed, tip electrodes are welded onto the signal leads. Springs, located outside of the hot area, put pressure on these alumina tubes, so that the point electrodes are pressed onto the top of the sample. The two point electrodes are used as voltage electrodes. Two platinum wires on the side make the connections to the current electrodes. The sample is placed on an alumina plate which is mounted on four outer steel tubes. All steel tubes are brazed together to form a rigid and electrically grounded construction which is attached to a brass head. A thermocouple for the measurement of the sample temperature is placed in one of the steel tubes. The brass head holds the BNC- and TRIAX-jacks as well as the inlet and outlet for the gas. A quartz tube, closed at one end, is fitted with an o-ring to the head
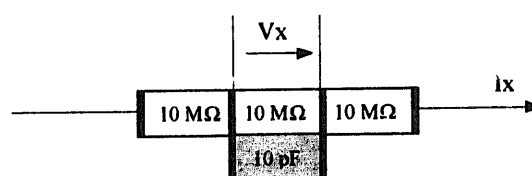

Fig. 6. Example of the arrangement of the calibration cell, consisting of SMD components.

of the holder. The holder is inserted into an electric furnace supplied by a dc power supply.

4. Calibration measuremenis and test of the performance

Test and calibration measurements were carried out on resistor–capacitor networks. Surface mount device (SMD) elements were used for these dummy cells. Normal resistors were too large and their geometry was not suitable for the measurement inside the sample holder in the four-probe set-up. Fig. 6 shows the cell arrangement for the calibration measurements. Three resistors of the same value are soldered together in series. A capacitor was soldered in parallel to the resistor in the centre in some cases. This dummy cell is shaped like a real sample and can be

mounted directly inside the holder. The outer terminals of this arrangement are connected to the current leads, the inner terminals to the voltage probes. In this configuration the performance of the whole set-up, arranged as in the experiment, can be checked.

The ac voltage level of the generator was between 10 mV_p and 1000 mV_p in all the calibration measurements. Distortion of the output signal of the amplifiers appeared at high frequencies at higher voltages. This can be explained by the disagreement between the large- and small-signal frequency response performance of the amplifier. The voltage gain of 100 V/V was used for the measurement of the 1 Ω and 100 Ω resistor and 1 V/V in the other cases. The current range was set between 10^3 V/A and 10^8 V/A, depending on the resistor to be measured. For the measurement of the impedance of the open holder, the voltage leads were connected to the current leads
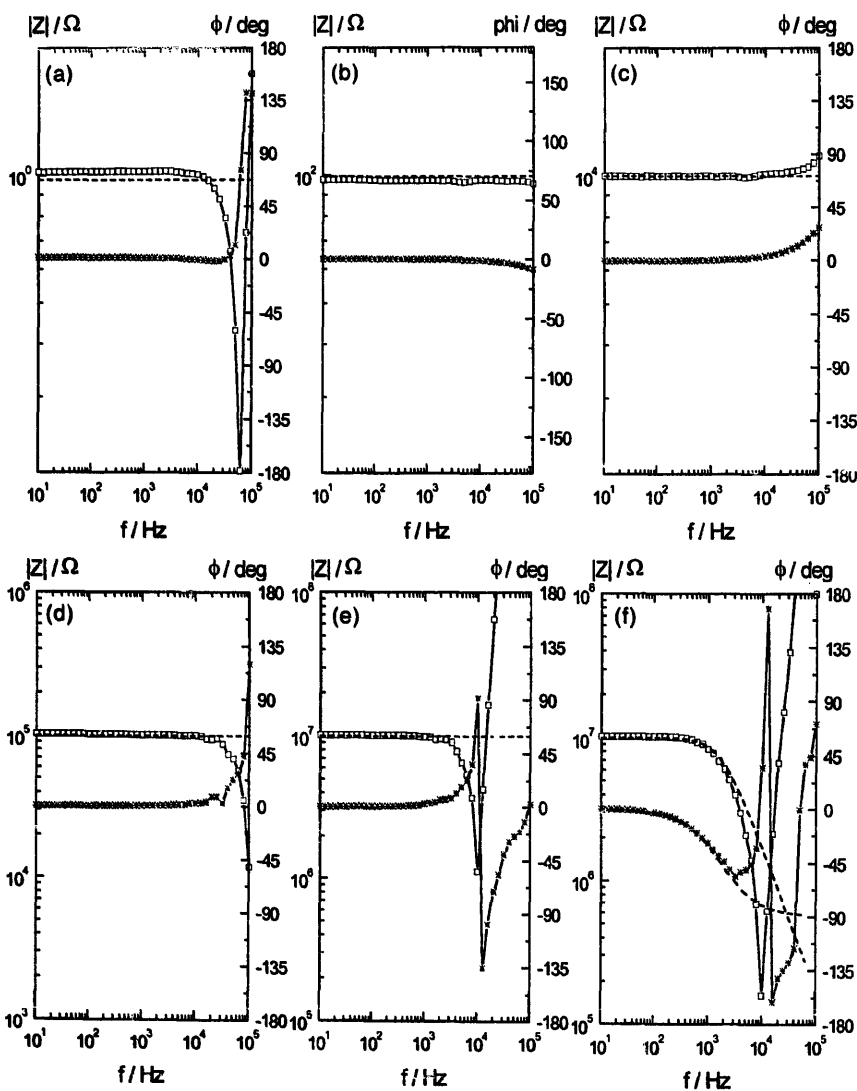

Fig. 7. Bode plot of different resistor values measured in the four-probe arrangement shown in Fig. 6. Squares indicate the absolute value, stars the phase angle, dashed lines the resistor values measured with the source measure unit Keithley SMU 237. (a) 0.976 Ω, $A_i = 10^3$ V/A, $A_u = 100$ V/V. (b) 99.38 Ω, $A_i = 10^3$ V/A, $A_u = 100$ V/V. (c) 9.994 kΩ, $A_i = 10^3$ V/A, $A_u = 1$ V/V. (d) 99.13 kΩ, $A_i = 10^5$ V/A, $A_u = 1$ V/V. (e) 9.997 MΩ, $A_i = 10^7$ V/A, $A_u = 1$ V/V. (f) 9.997 MΩ//9.2pF, $A_i = 10^7$ V/A, $A_u = 1$ V/V. Dashed lines in (f) represent the calculated values of the parallel circuit: 9.997 MΩ//9.2 pF.
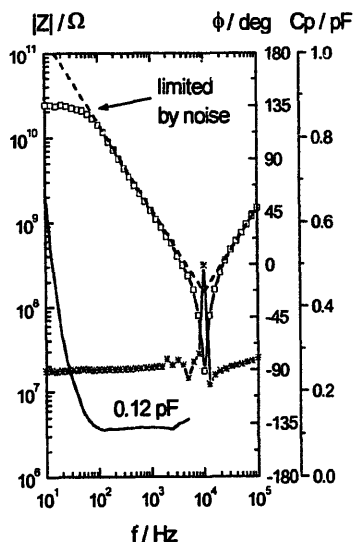
Fig. 8. Open holder, current and voltage electrodes directly connected. $A_i = 10^8$ V/A, $A_u = 1$ V/V. Solid line represents the calculated capacity of the open holder $C_{in} = 0.12$ pF.

directly. Therefore, the current through the voltage amplifier plus that through the geometric capacity was measured by the current amplifier. The results of the calibration measurements are presented in Figs. 7 and 8.

The measurements of the 1 Ω and the 100 Ω resistor show the sum of the frequency responses of the voltage amplifier with gain 100 V/V plus that of the current amplifier at a gain of 10^3 A/V. With the 10 kΩ resistor the voltage amplifier has a gain of 1 V/V and its widest bandwidth. Therefore, the frequency response characteristic of the current amplifier, at the gain 10^3 V/A, determines the measured values. At higher current gain ($A_i = 10^5$ for $R_x = 100$ kΩ) the bandwidth of the current to voltage converter becomes smaller. Gain peaking with a

peak frequency at approximately 100 kHz determines the upper frequency limit. With an amplification of 10^7 A/V the peak frequency is shifted down to approximately 10 kHz. This is in full agreement with the proposed origin of the peaking effect. The characteristic frequency of the low pass, f_{RC}, formed by the feedback resistor and the input cable capacitor in the current range of 10^7 A/V is one hundred times smaller than in the range 10^5 A/V. Together with the unity gain frequency, f_u, of the amplifier (1–2 MHz for the OPA128) the peak frequency can be calculated as the geometric mean of the unity gain frequency and the characteristic frequency of the low pass:
$$f_p = (f_u * f_{RC})^{-1/2} \text{ [10]}.$$

In the measurement of the open holder, the low frequency limit of about 200 Hz was determined by the signal to noise ratio of the current signal. Noise sources are the resistance noise and the voltage noise of the amplifier but there is no noise pickup from the power line because of the careful shielding. For an absolute value of the impedance higher than 10^{10} Ω and a current gain of 10^8 V/A at a generator signal amplitude of 100 mV$_p$, the current signal is only 1 mV$_p$. This signal level is usually too small, compared to the noise level, for measurements without special treatment, such as long integration time. The maximum absolute value of the impedance which can be measured is therefore approximately 10 GΩ. The high frequency limit appears at 2 kHz because of the gain peaking of the current amplifier and the following -40 dB/dec slope in its gain–frequency dependence. Therefore, in the Bode plot of the measured impedance, a minimum at 10 kHz and an increasing part afterwards with a slope of $+20$ dB/dec can be seen. At frequencies higher than approximately 50 kHz the low pass behaviour of the voltage amplifier starts to have an influence and the slope of the measured impedance becomes slightly smaller. The calcu-
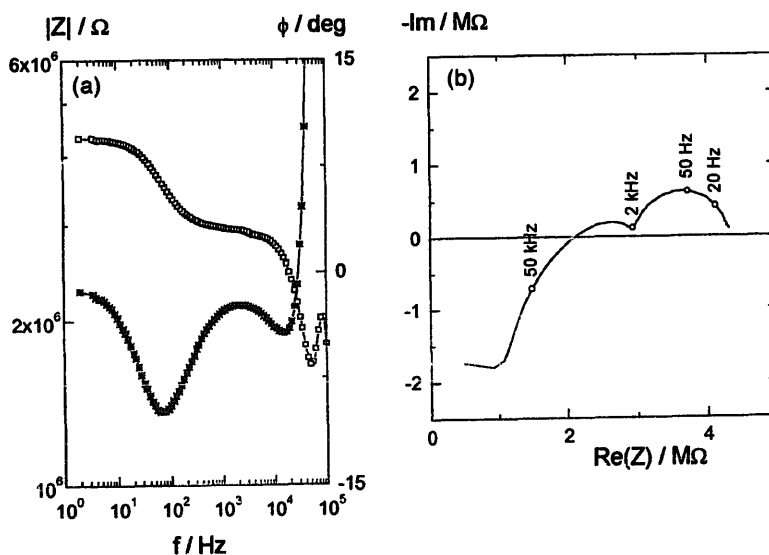

Fig. 9. Four-probe impedance of YSZ measured in air at 300°C. The total bulk resistance $R_b = 4.32$ MΩ. (a) Bode plot, squares = absolute value; stars = phase angle. (b) Nyquist plot.
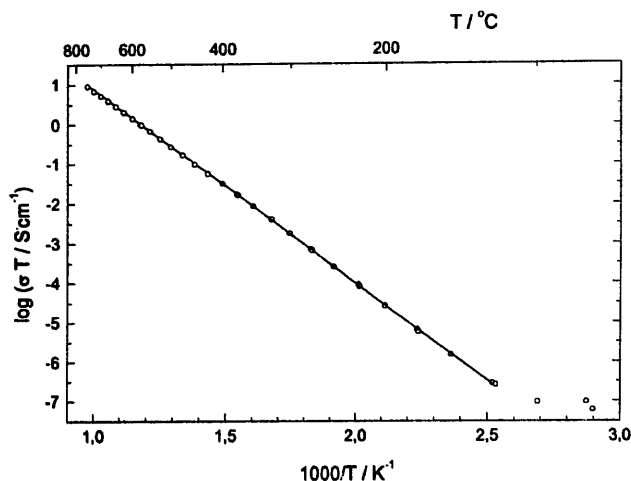
Fig. 10. Arrhenius plot of the total conductivity of YSZ. Solid line = linear regression. The activation energy was calculated to be $E_a = 0.97$ eV. Deviations at 100°C and 50°C from the straight line are caused by the noise limit of the measurement.

lated total input capacity C_{in}, which is the sum of input capacity of the amplifier and the geometric capacity, is only 0.12 pF.

A correction of the measured impedances, for the frequency response characteristics of the amplifiers is only reasonable for samples with low impedance. In high impedance systems, unpredictable errors from the 'outside' bulk impedance and interfacial impedance of the current electrode, as well as the impedance of the interface bulk|voltage electrode, together with the impedance of the voltage leads, will affect the impedance, Z_x, to be measured (see Fig. 2). Although the frequency and impedance range is extended because of the measuring principle, a correction will fail in many cases.

5. Measurements on YSZ

Ac four-probe impedance spectra were taken on polycrystalline yttria stabilised zirconia (YSZ) samples with 8 mol% yttria content (Degussit FZY from Trentini). The total bulk conductivity of YSZ strongly depends upon temperature, with an activation energy of about 1 eV. Therefore, the resistance of the sample at room temperature has values comparable to that of insulators.

Experiments were performed on rectangular cells with the size of $0.92 \times 0.475 \times 0.12$ cm in air. The samples were polished using SiC paper up to grade 1200. The current electrodes were gold films painted on the two opposite small sides. Voltage electrodes were applied in the same way on one large side of the sample with a distance of 0.5 cm from each other and a width of less than 0.1 cm. The use of point electrodes for the voltage probes is not feasible because of their high interfacial impedance. The electrodes were sintered in air at approximately 800°C. Spectra were taken every 50°C between room temperature and 750°C during heating and in the cooling cycle. Frequencies between 10 Hz and 100 kHz with a signal amplitude between 100mV and 1000 mV were set by a signal generator. The use of a more modern Frequency Response Analyser for the current and voltage signals would extend the lower frequency limit. A Bode and a Nyquist plot are shown in Fig. 9 as an example. The positive imaginary part at high frequencies results from the inadequate frequency response of the current amplifier above the bandwidth limit (see also Fig. 7). The conductivity of the sample was determined from the spectra by graphical extrapolation.

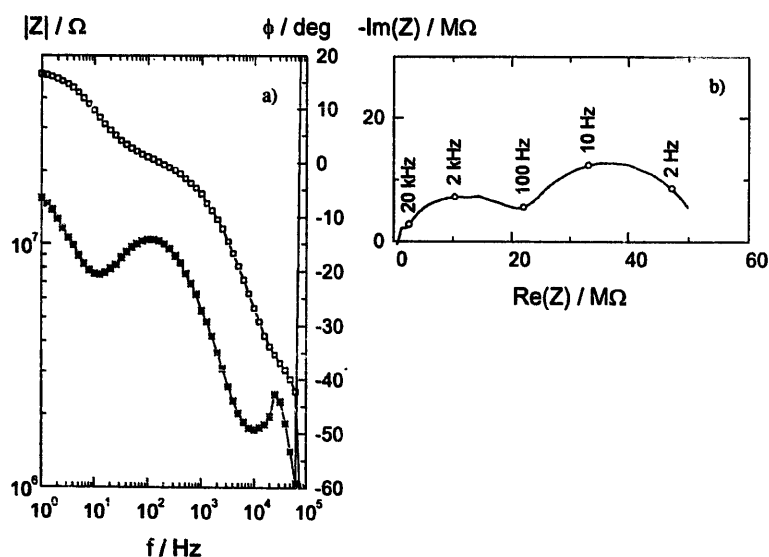Reproducible straight lines were obtained in the Arrhenius plot between 150°C and 750°C (Fig. 10). A deviation

Fig. 11. Four-probe impedance of BICUVOX.10 measured in air at 48.2°C. (a) Bode plot, squares = absolute value; stars = phase angle. (b) Nyquist plot.

from this straight line can be seen at lower temperatures. The impedance measured at this temperature was larger than 10 GΩ and therefore in the signal to noise ratio limit. At room temperature, the voltage amplifier ran into saturation because of the blocking behaviour of the voltage electrodes. This marks the absolute limit for all four-probe measurements even at fixed low frequencies or with dc methods.

6. Measurements on BICUVOX.10

BICUVOX.10 is the designation of the oxygen ion conductor $Bi_2V_{0.9}Cu_{0.1}O_{5.35}$ [11]. A polycrystalline sample of BICUVOX.10 was cut into a rectangular piece and polished with SiC paper up to grade 1200. The size of the sample was 0.8 $\times$ 0.475 $\times$ 0.18 cm. A thin film was painted with gold paste on the two opposite small sides for the current electrodes. The electrodes were sintered in air at 700°C. The platinum tip electrodes of the holder were attached directly to the sample in the first experiment. The distance between the point contacts was 0.23 cm. Impedance spectra were taken every 25°C from room temperature to 725°C and back. Frequencies between 1 Hz and 100 kHz with signal levels between 100 mV and 2000mV were applied.

In a second experiment the sample holder was placed in a Dewar bottle filled with liquid nitrogen. A heating coil allowed the control of the sample temperature between −150 and +200°C. In the first run below room temperature we saw that the voltage electrodes became blocking very early. Therefore voltage electrodes were applied with platinum paste and sintered in air at 700°C. The distance between the voltage electrodes was 0.23 cm and their width was less than 0.05 cm. The measurement could be extended to −15°C with that type of electrode before the interfacial impedance became too large. The measurements
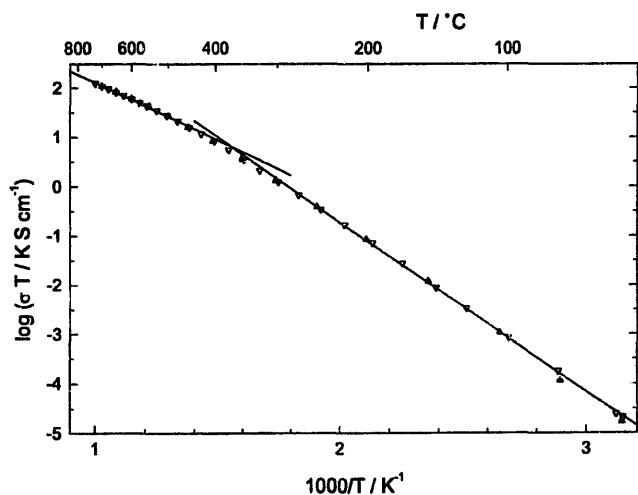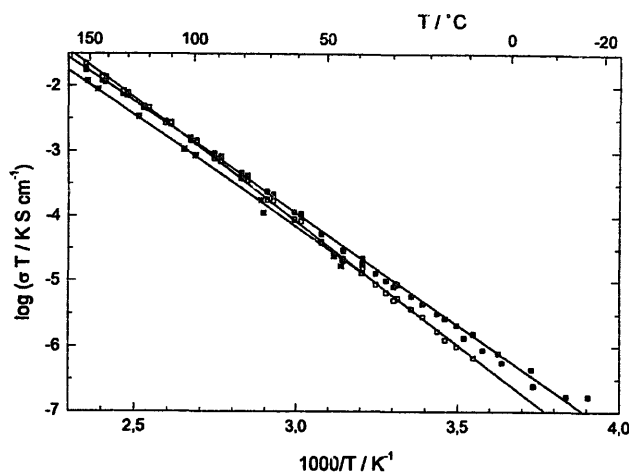
Fig. 13. Arrhenius plot of the conductivity of BICUVOX.10, low temperature measurement. $\square$ = grain boundary; $\blacksquare$ = grain interior; stars = total conductivity of the high temperature measurement; solid line = linear regression.

were performed from room temperature to 150°C and back with steps of 10°C. A cooling cycle with 5°C steps down to −30°C and again a heating/cooling cycle with a maximum temperature of 150°C followed. The Nyquist plot (Fig. 11b) shows two well separated semi-circles in a very restricted temperature range from 25°C to 100°C, because of our relatively small frequency window of 1 Hz to about 100 kHz. The interceptions with the real axis at high and low frequencies were interpreted as grain interior resistance, R_g, and the total bulk resistance, which is the sum of R_g and the grain boundary resistance, R_{gb}, respectively. Above 200°C the frequency dependence of the impedance displays pure Ohmic behaviour up to the high frequency limit of our instrument. This value corresponds to the total bulk resistance. The bulk conductivity is shown in an Arrhenius plot for the high temperature experiment (Fig. 12). The temperature dependence of the grain interior and grain boundary conductivity is plotted in Fig. 13 for the low temperature experiment. The bulk conductivity of the first experiment is also shown for the overlapping temperature range in that diagram. The agreement of the activation energies and conductivity values with previous results from two-probe impedance measurements [12] is good (Table 1). The limit of the instrument was achieved at −15°C by the saturation of the inputs of the voltage amplifier.

Fig. 12. Arrhenius plot of the total conductivity of BICUVOX.10, high temperature measurement. $\blacktriangle$ = heating cycle; $\triangledown$ = cooling cycle; solid line = linear regression.

Table 1
Comparison of activation energies of BICUVOX.10 obtained by four-probe and two-probe impedance spectroscopy

	Temperature range (K)	E_a (eV) This work	[12]
Total bulk conductivity	> 750	0.476	0.481
Total bulk conductivity	< 730	0.681	0.682
Grain interior		0.68	0.643
Grain boundary		0.751	0.75

References

[1] W.I. Archer, R.D. Armstrong, Specialist Per. Report, The Chemistry Society London, Electrochemistry I (1980) 157.

[2] P. Linhardt, M. Maly-Schreiber, M.W. Breiter, in: F.W. Poulsen, N. Hessel Henderson, K. Clausen, S. Skaarup, O. Toft Sorensen (Eds.), Proc. 6th Int. Symp. on Metallurgy and Materials Science, RISO National Laboratory, Roskilde, 1985, p. 475.

[3] S.P.S. Badwal, F.T. Ciacchi, D.V. Ho, J. Appl. Electrochem. 21 (1991) 721.

[4] J.J. Bentzen, N.H. Andersen, F.W. Poulsen, O.T. Sorensen, R. Schram, Solid State Ionics 28-30 (1988) 550.

[5] C. Gabrielli, Schlumberger Technologies, technical report, 1990.

[6] J.R. Dygas, M.W. Breiter, Electrochim. Acta 41 (1996) 993.

[7] J.A. Chroboczek, J. Link, J. Phys. E Sci. Instrum. 18 (1985) 568.

[8] Keithley, Low Level Measurements, 1992.

[9] Burr Brown, IC Data Book, Linear Products, 1994.

[10] Burr Brown, Applications Handbook, 1994, pp. 172-206.

[11] F. Abraham, J.C. Boivin, G. Mairesse, G. Novogrocki, Solid State Ionics 40/41 (1990) 934.

[12] J.R. Dygas, F. Krok, W. Bogusz, P. Kurek, K. Reiselhuber, M.W. Breiter, Solid State Ionics 70/71 (1994) 239.